Pressure dependent kinetic analysis of pathways to naphthalene from cyclopentadienyl recombination

Pressure dependent kinetic analysis of pathways to naphthalene from cyclopentadienyl recombination

Alan E. Long[a], Shamel S. Merchant[a], Aäron G. Vandeputte[a], Hans-Heinrich Carstensen[b]
Alexander J. Vervust[b], Guy B. Marin[b], Kevin M. Van Geem[b], William H. Green[a]✉

[a] *Department of Chemical Engineering, Massachusetts Institute of Technology, 77 Massachusetts Ave., Cambridge, MA 02139, USA*

[b] *Laboratory for Chemical Technology, Ghent University, Technologiepark 914, B-9052 Gent, Belgium*

✉ corresponding author. E-mail: whgreen@mit.edu Phone: (617) 253-4580
Post: 77 Massachusetts Ave., Cambridge, MA 02139

Article Type: Full-length
Running Title: Pressure dependent analysis: CPDyl to $C_{10}H_8$

Abstract

Cyclopentadiene (CPD) and cyclopentadienyl radical (CPDyl) reactions are known to provide fast routes to naphthalene and other polycyclic aromatic hydrocarbon (PAH) precursors in many systems. In this work, we combine literature quantum chemical pathways for the CPDyl + CPDyl recombination reaction and provide pressure dependent rate coefficient calculations and analysis. We find that the simplified 1-step global reaction leading to naphthalene and two H atoms used in many kinetic models is not an adequate description of this chemistry at conditions of relevance to pyrolysis and steam cracking. The $C_{10}H_{10}$ species is observed to live long enough to undergo H abstraction reactions to enter the $C_{10}H_9$ potential energy surface (PES). Rate coefficient expressions as functions of T and P are reported in CHEMKIN format for future use in kinetic modeling.

***keywords*:** polycyclic aromatic hydrocarbons (PAH) · cyclopentadiene · naphthalene · pressure dependent kinetics

1 Introduction

Polycyclic aromatic hydrocarbons (PAHs) are a class of molecules comprised of hundreds of chemicals produced from various anthropogenic sources, such as the incomplete combustion of fuels in boilers and heating devices, oil refining processes, and the combustion of transportation fuels (in particular diesel). Many PAHs are known to be carcinogenic or mutagenic as well as important precursors to soot[1–5]. Increasing energy demands and more stringent emission regulations have spurred research into various new technologies that reduce PAH emissions[6–8]. Despite the attention that these PAHs have attracted, many questions related to their formation remain not fully understood, i.e. what are the key reactions responsible for the formation of PAHs and what are the main PAH precursors? Researchers have developed extensive kinetic mechanisms describing low and high temperature fuel oxidation, but few exist that are able to predict the PAH growth and subsequent soot formation[9–11]. Some key efforts toward the latter have come from Frenklach, Appel et al., and Richter and Howard[12–15]. However, these studies focused primarily on the chemistry at high temperature flame conditions, at which the HACA mechanisms first proposed by Frenklach in 1991 as well various similar pathways summarized in the review article by Richter and Howard[12,14] dominate. The radicals involved in these reactions are highly reactive or energetic and thus not present in sufficient concentrations at lower temperatures. Given their increased stability, resonantly stabilized radicals such as allyl, propargyl and cyclopentadienyl (CPDyl) have been suggested as possible precursors of aromatic products at low or moderate temperatures[16–19]. However, most of these reactions lead to mono-aromatic hydrocarbons. Several experimental pyrolysis studies at lower temperatures detected CPD as an important product and Melton et al. showed that PAH formation was most sensitive to the CPD concentration[20–23]. Since CPD is easily converted to CPDyl this suggests that CPDyl radicals play a crucial role in PAH formation. In this work, the focus is on the development of a detailed kinetic network for cyclopentadienyl recombination that is relevant at pyrolytic and low-temperature combustion conditions to describe the formation of naphthalene, the simplest PAH and an important PAH precursor.

As briefly indicated above, a number of researchers have explored the thermal decomposition of CPD experimentally. In an attempt to obtain bond dissociation energies, the decomposition of CPD under pyrolytic conditions was studied by Szwarc in 1950 [24]. This led to a complicated decomposition spectrum, containing H_2, CH_4, C_2 hydrocarbons and other

species hinting at the complexity of the CPD reaction network. In 1972 Spielman and Cramers first proposed a potential role of CPD in the formation of the initial aromatics, observing products such as styrene, indene, and naphthalene under pyrolytic conditions[25]. This was then validated by studies of the pyrolysis and hydrogenolysis of phenol[26–28]. Burcat et al. studied the high-temperature decomposition reactions of CPD in a shock-tube in 1996, and modeled it with a simple model of 36 reactions. Roy et al. also studied CPD reactions using shock tube experiments and reported rate coefficients for the C–H bond scission and the reaction between CPD and a hydrogen atom[29,30]. While the Spielman study and others showed qualitatively that naphthalene appears to be produced from CPD, in 2003, Murakami et al. first experimentally derived a rate expression for a net reaction from CPDyl to naphthalene, assuming CPD initially forms its relatively stable radical [31]. More recently, experimental efforts to understand CPD pyrolysis chemistry have shifted toward flow reactor studies[32,33]. Djokic et al. and Kim et al. identified and quantified numerous pyrolytic products from CPD up to anthracene, phenanthrene and fluorene supporting the important role of CPD and CPDyl in PAH formation. The crucial role of CPDyl radicals in PAH formation is additionally confirmed by pyrolysis studies of anisole (which forms CPDyl by methyl loss and carbon monoxide ejection) and dimethylfuran[20,34,35]. More recently, in 2015, Knyazev and Popov experimentally investigated the total self-reaction rate of CPDyl, finding it to show significantly faster kinetics when compared with other similar radical self-reactions. Naphthalene and Azulene were detected as final products with the former being the major product [36].

The first quantum chemical exploration of the potential energy surface (PES) for CPDyl recombination was reported by Melius et al. in 1996. This study used the BAC-MP4 and MP2 levels of theory to characterize pathways in which two CPDyl radicals recombine, subsequently lose an H atom to form a fulvalanyl radical (Figure 1), which then isomerizes and ejects an additional H atom to yield naphthalene. The importance of hydrogen atom mobility for PAH formation was emphasized by this work as was the role of resonantly stabilized intermediates[37]. A 2006 paper by Wang et al. extended the surface using the B3LYP level to incorporate pathways to benzene and indene as well as naphthalene. However, that work focused on initial reactions between CPD and CPDyl rather than two CPDyl radicals. It was observed that C-C β scission routes tended to be favored at high temperatures[38]. A 2007 paper by Kislov and Mebel used the RCCSD(T)/6-311G(d,p) level to investigate the $C_{10}H_9$ potential energy surface. Routes to naphthalene, azulene, and

fulvalene were compared. Assuming unimolecular reaction in the high pressure limit, fulvalene was computed to be the dominant product above 1500 K, while naphthalene was the primary species at lower temperatures, and azulene was always a minor product. Kislov and Mebel extended their work in 2008 to incorporate the relevant portion of the $C_{10}H_{11}$ surface consisting principally of routes to indene calculated at the G3 level[39]. Subsequent work by Kislov and Mebel elucidated the poor likelihood of reaction pathways that would produce molecular hydrogen along the way to naphthalene from two CPDyl radicals as had been proposed as a global step for the pathway and incorporated into some kinetic mechansims[40,41]. A 2012 paper by Cavallotti et al. revisited routes from the reaction of CPD with CPDyl using the B3LYP level for most calculations and ROCBS-QB3 for important flux determining steps along the pathways analyzed. Additional routes were located for the formation of indene, benzene, vinylfulvene, and phenyl butadiene[42]. In 2013 Cavallotti et al. analyzed the $C_{10}H_{10}$ surface at the CBS-QB3 level, focusing on the formation of the fulvalanyl and azulanyl radicals. Routes to the azulanyl radical were reported to dominate up to 1450K[43]. This result in turn added relevance of the spiran and methyl walk pathways from azulene to naphthalene shown by Alder et al. in 2003[44]. Some additional discussion of many of these quantum chemical studies can be found in a recent paper by Mebel et al.[45].

Rate coefficients are needed to quantitatively model PAH formation kinetics. A number of the previously noted studies presented high pressure limit rate coefficients and global step rate constants. Wang et al. reported only high-pressure limit Arrhenius expressions for the primary reaction pathway branching reactions they studied[38]. The 2007 and 2008 Kislov and Mebel papers reported rate coefficients and equilibrium constants for all important reactions they located. These were reported at various relevant temperatures in table format[39,46]. Global overall Arrhenius expressions were reported by Cavallotti et al. in 2012 and 2013 for the formation of the terminal species of interest in those studies[42,43]. However, none of these studies incorporated pressure dependence in their reported rate expressions. While the C_{10} species of interest are relatively large molecules, they are not large enough to be sure their unimolecular reactions are at the high pressure limit at pyrolysis and combustion conditions. This follows from a 2003 paper by Wong et al. which developed convenient criteria for determining the relevance of pressure dependent kinetics for a system[47]. Following this criteria, a recent model of propene pyrolysis includes a set of pressure dependent rate expressions for the progression of CPDyl to naphthalene first

described by Melius et al. Rather than calculating the individual rates for the network directly, they are assigned based on analogy to similar reaction whose rate constants readily available [48]. A brief comparison with this estimated network is presented in the supporting information of this work.

The objective of the current study is two-fold. First it aims to combine the most promising pathways previously studied and use this information to calculate a set of pressure-dependent rate expressions that will be easily used in future kinetic mechanisms. Specifically, generation of rate expressions in this format is important for database development and improved accuracy of automatic mechanism generating software such as RMG[49]. Secondly, the importance of the direct channel

$$\text{CPDyl} + \text{CPDyl} \rightarrow \text{naphthalene} + 2\ \text{H} \qquad \Delta_r H^{298} = 48\ \text{kJ/mol}$$

will be explored. Note that as written, the recombination of CPDyl radicals generates naphthalene in a single step, preventing any bimolecular chemistry of intermediates in this obviously complex reaction sequence. Also, it increases reactivity by converting two low-reactivity radicals into more reactive H atoms.

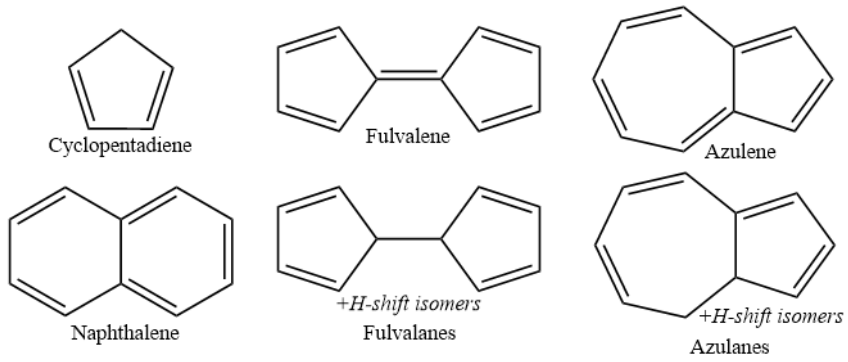

Figure 1: *Primary structures of this study. An ending of –yl added to a species indicates a radical of that species formed by hydrogen loss.*

2 Methodology

Quantum mechanical calculation of PES. Even though all PES used in this study have already been investigated previously by other groups, the electronic structure calculations are repeated here to obtain a consistent data set for the kinetic analysis. Thermodynamic properties of all species including transition states are calculated using quantum mechanical computations at the CBS-QB3 level as implemented in Gaussian 03 and 09[50–53]. Bond additivity and spin orbit corrections are included[54,55]. Most vibrations are approximated as

harmonic oscillators with frequencies computed at the B3LYP/6-311G(2d,d,p) level, but torsional vibrations of key components are treated as 1D hindered rotors[56]. The calculated CBS-QB3 enthalpy of formation of CPDyl at 298K is 259 kJ/mol in good agreement with the experimental value[29]. The optimized geometries for all species studied here are readily available in previous PES exploratory studies as referenced.

Rate coefficient calculations. For pressure dependent calculations, potential energy surfaces for $C_{10}H_{10,}$ and $C_{10}H_9$ are modeled using a one-dimensional master equation, accounting for rotational degrees of freedom. Microcanonical rate coefficients are computed using the classical RRKM theory and include Eckart tunneling contributions[57–60]. Densities of states are calculated via inverse Laplace transform of the partition function using the method of steepest descents[61–63]. Phenomenological rate coefficients (which give the dynamics of the total isomer populations $x_i(t)$) are computed from the conventional master equation model (which give the detailed dynamics of the isomer population distributions $p_i(E_n,t)$) using the modified strong collision (MSC) approximation[64,65]. Parameters for the MSC calculation are obtained using the exponential down model $\langle\Delta E_{down}\rangle$ for the average energy transferred in a collision, which is subsequently converted to the required ΔE_{all} parameter[64]. The average downward energy transfer per collision is calculated according to the following temperature dependent formulation:

$$\left\langle \Delta E_{down} \right\rangle = \left\langle \Delta E_{down} \right\rangle_{300} \left(\frac{T}{300\ \mathrm{K}} \right)^{n} \mathrm{cm}^{-1}$$

with $\langle\Delta E_{down}\rangle_{300}$ = 295 cm^{-1}, and n = 0.7 for N_2. These values are adopted based on azulene collisional energy transfer parameters[66]. The collision frequency is computed by assuming a Lennard-Jones potential between the bath gas and the species of interest. Lennard-Jones parameters are approximated by first estimating the critical temperature and pressure using a group additivity method devised by Joback, and then using the equations for a Lennard-Jones gas implemented by Harper et al. in RMG [67–69]. All master equation calculations are performed using the open source CANTHERM software package[70]. Additionally, barrierless hydrogen loss reactions are assumed fast and temperature independent with high pressure limit rate coefficients of $1 \times 10^{14}\ \frac{cm^3}{mol\ s}$ in the recombination direction for the purposes of this study. This estimate is in agreement with the 2005 Harding et al. work computing the rates of a variety of hydrogen atom-hydrocarbon radical recombination rates.

These rates were shown to vary less than one order of magnitude from the value assumed here. [71]. For the CPDyl + CPDyl association rate, the high pressure limit rate expression from Knyazev and Popov is used. This value was determined experimentally for a range of 300-600K [36]. Sensitivities for these assumed rates are included in the supporting information.

3 Results and discussion

3.1 $C_{10}H_{10}$ PES to Fulvalanyl and Azulanyl Radicals

A schematic of the overall $C_{10}H_{10}$ surface examined in this study is shown in Figure 2. More detailed enthalpy diagrams will be shown in later figures which give the individual structures, but divide the PES into two parts due to the large number of species. When entering the isomerization network through the combination of two CPDyl radicals, the initial adduct has a number of options to further react. First, it can immediately stabilize via collisions and energy transfer to surrounding molecules, thermalizing it to one of the fulvalane species. Based on the energies and barriers, this is expected to be the dominant channel at sufficiently high pressure. Secondly, if the combination of CPDyl radicals produces an adduct with sufficient excess energy, it may be able to rearrange and pass over the high barrier separating the fulvalanes and azulanes before being collision stabilized. Entering the PES at even higher energy levels allows for skipping over the wells of the $C_{10}H_{10}$ PES entirely, emitting a hydrogen radical and proceeding immediately to the $C_{10}H_9$ PES related to fulvalanyl or azulanyl. While a larger degree of atomic rearrangement is necessary to proceed directly to azulanyl, those species are of lower energy than the fulvalanyl isomers. It may thus be possible at certain conditions to generate preferentially azulanyl radicals. Once a fulvalanyl or azulanyl radical has been formed, the $C_{10}H_9$ species can isomerize or eliminate an H atom to form naphthalene, fulvalene, or azulene, Figure 7.

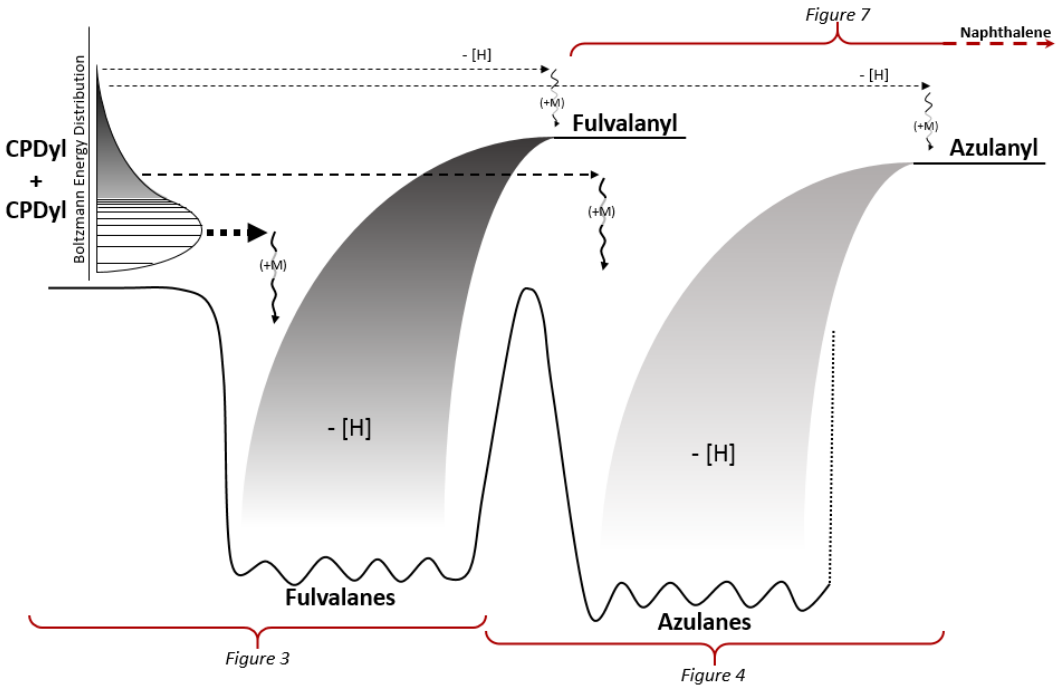

Figure 2: *$C_{10}H_{10}$ surface schematic. The azulanes fall slightly lower in energy than the fulvalanes with an isomerization barrier separating the two groups of roughly equal height to the entrance channel. Due to the number of species, the surface has been broken into several figures as indicated for display purposes, but note that the calculations are performed on the surface as a whole.* [Color: web only]

Fulvalanyl radical formation: The CPDyl radical recombination reaction and subsequent $C_{10}H_{10}$ surface was first examined by the 1996 work by Melius et al., but that work considered only three of the six potential $C_{10}H_{10}$ H-shift isomers and neglected one of the three fulvalanyl radical isomers[37]. The complete set of isomers was later shown by the 2013 Cavallotti et al. work[43]. The results of our study show that all wells (isomers) are important and isomerization pathways must be included in the kinetic analysis since missing low-barrier sigmatropic hydrogen shift reactions and isomers will under-predict the total yield of $C_{10}H_{10}$ isomers formed in the recombination reaction. A reduced build-up of $C_{10}H_{10}$ isomers will lead to an underestimation of naphthalene and other species produced through H loss pathways from these isomers.

The fulvalane/fulvalanyl portion of the network is shown in Figure 3. The six fulvalane isomers (**T1a** to **T1f**) can easily interconvert due to the relatively low barriers for the sigmatropic H shifts in these components. The CBS-QB3 method predicts barriers that are in the range of 90-120 kJ mol^{-1}. This agrees well with previous computational results[37,43]. The isomers with co-planar conjugated rings (**T1c**, **T1d** and **T1e**) are significantly more stable than other isomers. The lowest barrier hydrogen emission occurs between **T1b** and **N1b** at

270 kJ/mol. In general, the C–H bond dissociation energies (BDE) of **T1a** to **T1f** range between 270 and 330 kJ/mol^{-1}, much smaller than C-H bond energies in alkanes which are around 400 kJ mol^{-1} and still lower than the allylic C-H bond energy in propene (about 370 kJ mol^{-1}) [72].

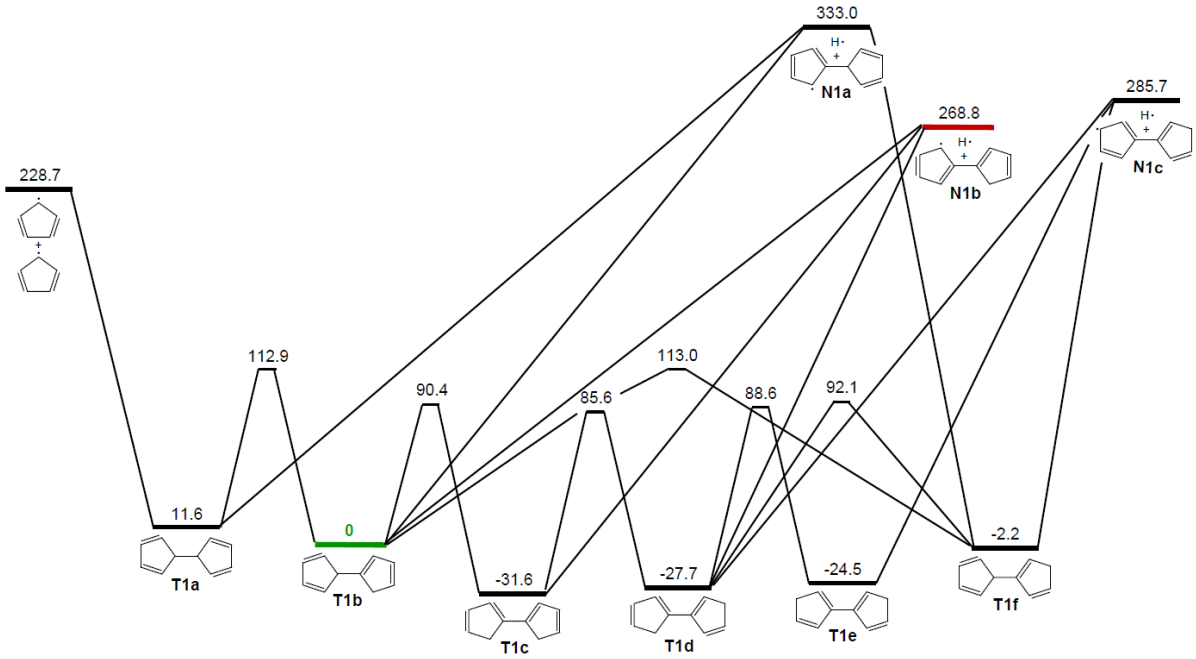

Figure 3: *CBS-QB3 enthalpy diagram H(0 K) (kJ/mol) for the $C_{10}H_{10}$ surface initiated by the recombination of two CPDyl radicals. All enthalpies are relative to the adduct T1b which connects to the other portion of the surface. This network was first reported by Melius et al. and in its complete form by Cavallotti et al.*[37,43] [Color: web only]

Azulanyl radical formation: The pathway used for this study (Figure 4) was first discussed by Cavallotti et al. as being important at lower temperatures[43]. This is primarily due to the increased stability of the azulane species (**T4a** to **T4d**). Possible reaction pathways to azulanyl radical were also explored by Kislov and Mebel, though their work examined channels on the $C_{10}H_9$ surface[39,43].

The portion of the surface relevant for azulanyl radical formation is shown in Figure 4 and begins with species **T1b** from Figure 3. Similar to the formation of fulvalanyl the path is relatively simple, passing through a tricyclic species (**T2**) followed by a ring opening (**T3**) and closing to form the azulane species. The azulane species are interconnected by various hydrogen shift reactions. The H-shifts barriers for the azulane species range from around 100-150 kJ/mol indicating a greater resistance to interconversion than is observed for the fulvalanyl species. The lowest energy route to the $C_{10}H_9$ surface requires an increase in

energy of 270 kJ/mol from a fulvalane isomer, about 5 kJ/mol less than any path from an azulane isomer. Though the separating barrier between the fulvalanes and azulanes is relatively high, it is still about 15 kJ/mol lower than the CPDyl + CPDyl entrance channel. Therefore, isomerization to the more stable azulane isomers is energetically feasible, suggesting that rather high azulane concentrations can build up at lower temperatures and thus subsequent azulane pathways need to be included. Three other symmetry allowed azulane species are included in the analysis and calculations for the $C_{10}H_{10}$ surface but are omitted from Figure 4 since they are only accessible by traversing a 70 kJ/mol higher barrier from **T4a**.

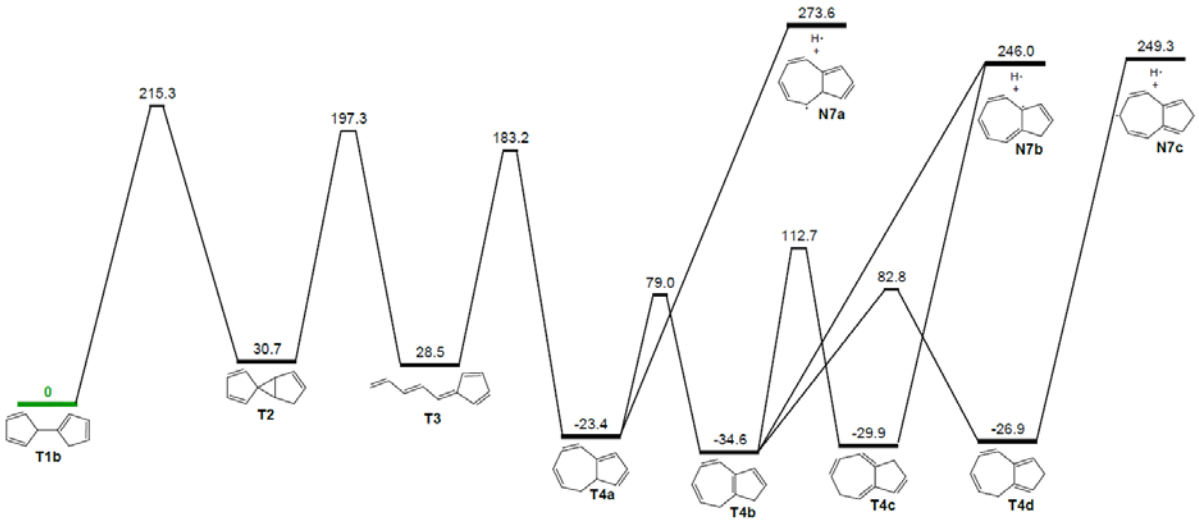

Figure 4: *CBS-QB3 enthalpy diagram H(0 K) (kJ/mol) on the $C_{10}H_{10}$ surface leading to the formation of Azulanyl radicals. All enthalpies are relative to component T1b which represents the dominant entrance channel. Pathway first shown by Cavallotti et al.*[43]. *Additional symmetry allowed azulane species were included in this analysis but are not shown in this figure for simplicity reasons as they are only accessible via a 170 kJ/mol barrier from T4a.* [Color: web only]

Some authors have treated this surface as if the chemically activated routes dominate, even so far as to use a single rate expression to describe the direct conversion from two CPDyl radicals directly to naphthalene and two hydrogen atoms[31]. Here evidence against the validity of this assumption is presented through calculation of the pressure dependent rate constants for this network. The resulting rate coefficients for the various reaction pathways of the recombination of two CPDyl radicals at 1100 K can be found in Figure 5a as functions of pressure. H atom forming channels are only of minor importance (< 1%) at all pressures investigated. Instead, collision stabilization leads to the formation of various fulvalane isomers. At pressures above atmospheric conditions (P>1 bar), the recombination reaction of the two CPDyl radicals results primarily in the formation of **T1a** and well-skipping reactions

are suppressed. Around 1 bar and below, well-skipping reactions become important and **T1c** becomes the dominant product. Therefore, at typical conditions the intermediate formed after recombination of two CPDyl radicals only slowly stabilizes, allowing the hydrogen atoms to freely move around in the molecule.

The direct and well-skipping rate coefficients, $k_{A \to B}(T,P)$, are displayed in matrix form in Figure 5b. The bottleneck is the conversion of the fulvalanes into species **T2**, which occurs on a millisecond timescale at 1100 K. Equilibration between the fulvalane species prior to the bottle neck occurs on a much faster microsecond time scale. While slower than the fulvalanes, the azulane species also interconvert rapidly.

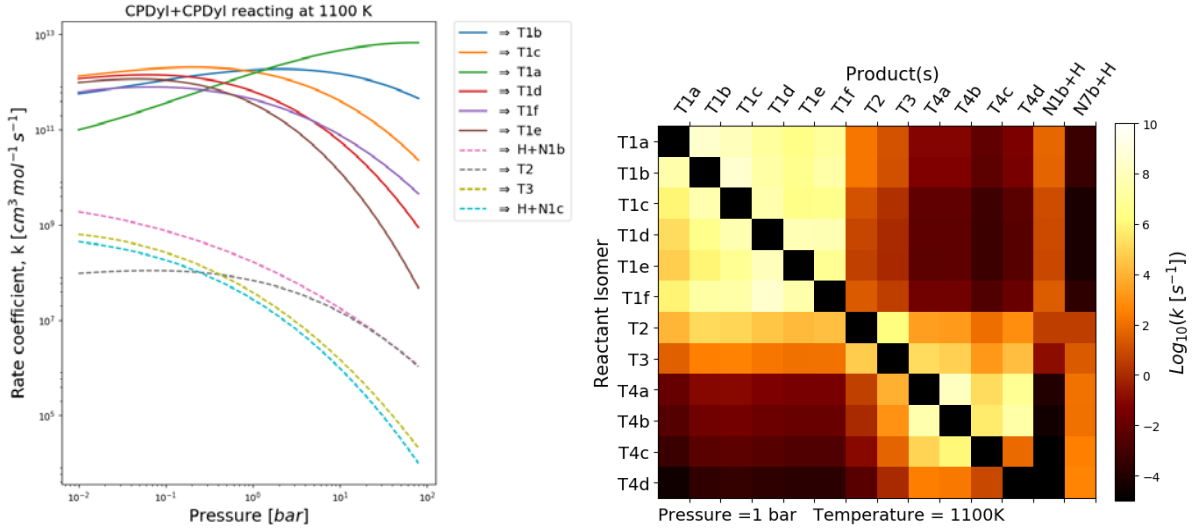

Figure 5*: (**A:** Left) Computed pressure dependent rate coefficients for the recombination of two CPDyl radicals to form various products in N_2 at 1100 K. The corresponding PES is shown in Figure 3 and Figure 4. (**B:** Right) Rate constant matrix depicting rate constant magnitudes for all well-skipping and direct reactions between isomers of the $C_{10}H_{10}$ PES. Reacting species shown on the y axis with the product species along the x axis.* [Color: web & print]

With pressure dependent rate analysis confirming that species are stabilized on the $C_{10}H_{10}$ surface and do not predominantly proceed directly to $C_{10}H_9$, it is thus possible that $C_{10}H_9$ formation occurs through three different paths: chemically activated hydrogen loss from the CPDyl reaction ($2CPDyl \rightarrow C_{10}H_9+H$), hydrogen emission from the $C_{10}H_{10}$ species ($C_{10}H_{10} \rightarrow C_{10}H_9+H$), and radical hydrogen abstraction from the $C_{10}H_{10}$ species ($C_{10}H_{10}+R\cdot \rightarrow C_{10}H_9+RH$). To see how the three pathways relate to one another, $C_{10}H_9$ formation rates are calculated for 1 and 100 bar, Figure 6. This is done by using the fastest rates to approximate the activated route ($2CPDyl \rightarrow N1b+H$) and the emission route (T1b → N1b+H), while estimating the rate of the hydrogen abstraction route as T1b + CPDyl → N1b+CPD using the Reaction Mechanism Generator (RMG) and its corresponding

database $\left(A = 1.1 \cdot 10^{-9} \frac{m^3}{mol\ s},\ n = 4.3,\ Ea = 48\ \frac{kJ}{mol}\right)$[49]. For concentrations, CPDyl is assumed in equilibrium with the $C_{10}H_{10}$ isomers since CPDyl is the starting species and the radical recombination reaction is fast. The total concentration of CPDyl + 2 $C_{10}H_{10}$ is constrained to $2 \cdot 10^{-9}\ \frac{mol}{cm^3}$ for all conditions to simplify the comparison. This concentration is obtained using simulation of CPD pyrolysis using the POLIMI 1311 mechanism at the low dilution conditions of Djokic et al. at 1000K [33]. See Table 1 for data used to generate Figure 6. For high temperatures, the chemically activated route to $C_{10}H_9$ + H plays a major role. Although $C_{10}H_{10}$ is the dominant product of recombination of the two CPDyl radicals, the subsequent thermal decomposition of the $C_{10}H_{10}$ isomers to $C_{10}H_9$ + H is predicted to play essentially no role in the formation of naphthalene. This is because $C_{10}H_{10}$ → CPDyl + CPDyl is energetically favored over $C_{10}H_{10} \rightarrow C_{10}H_9 + H$ (Figure 2).

Table 1: *Selected data set used for the rate analysis of $C_{10}H_9$ formation routes as shown in Figure 6.*

Pressure (bar)	1			100		
Temperature (K)	800	1000	1200	800	1000	1200
k $_{CPDyl + C_{10}H_{10} \rightarrow C_{10}H_9 + CPD}$ $\left(\frac{cm^3}{mol \cdot s}\right)$	3.5E+06	3.9E+07	2.2E+08	3.5E+06	3.9E+07	2.2E+08
k $_{2CPDyl \rightarrow C_{10}H_9 + H}$ $\left(\frac{cm^3}{mol \cdot s}\right)$	2.4E+06	5.1E+07	4.5E+08	3.2E+03	1.6E+05	3.0E+06
k $_{C_{10}H_{10} \rightarrow C_{10}H_9 + H}$ (s^{-1})	9.2E-10	2.8E-06	5.0E-04	1.2E-09	4.3E-06	9.8E-04
[CPDyl] $\left(\frac{mol}{cm^3}\right)$	1.0E-11	4.3E-10	1.9E-09	1.0E-11	4.3E-10	1.9E-09
[$C_{10}H_{10}$] $\left(\frac{mol}{cm^3}\right)$	9.9E-10	7.9E-10	6.0E-11	9.9E-10	7.9E-10	6.0E-11
[CPDyl] + 2[$C_{10}H_{10}$] $\left(\frac{mol}{cm^3}\right)$	2.0E-09	2.0E-09	2.0E-09	2.0E-09	2.0E-09	2.0E-09

At 1 bar the radical abstraction route from $C_{10}H_{10}$ to $C_{10}H_9$ becomes the dominant pathway below 1020K. The crossover temperature rises with pressure to 1230K at 100 bar. Therefore, radical hydrogen abstraction is particularly relevant at the conditions of pyrolytic experimental studies of CPD. Additionally, the range of relevance is expected to extend to higher temperatures if the full system radical pool is taken into account as possible abstractors rather than just CPDyl as is done here. The marked shifts in slope for each of the three curves is attributed to a shift in equilibrium to favor CPDyl over $C_{10}H_{10}$ as seen in Table 1. For temperatures above this point, CPDyl is the major species while $C_{10}H_{10}$ becomes the minor species and its concentration begins to fall at an increased rate. A figure showing this trend is included in supporting information. An important consequence of the observed importance of radical H abstraction is a shift in net 'radical' balance through the formation of naphthalene from CPDyl at these lower pyrolytic temperatures: "Two radicals in, two H atoms out" (when

the chemically activated channel dominates) becomes “three radicals in, one H atom out” at lower temperatures, causing potentially a marked reduction in system reactivity.

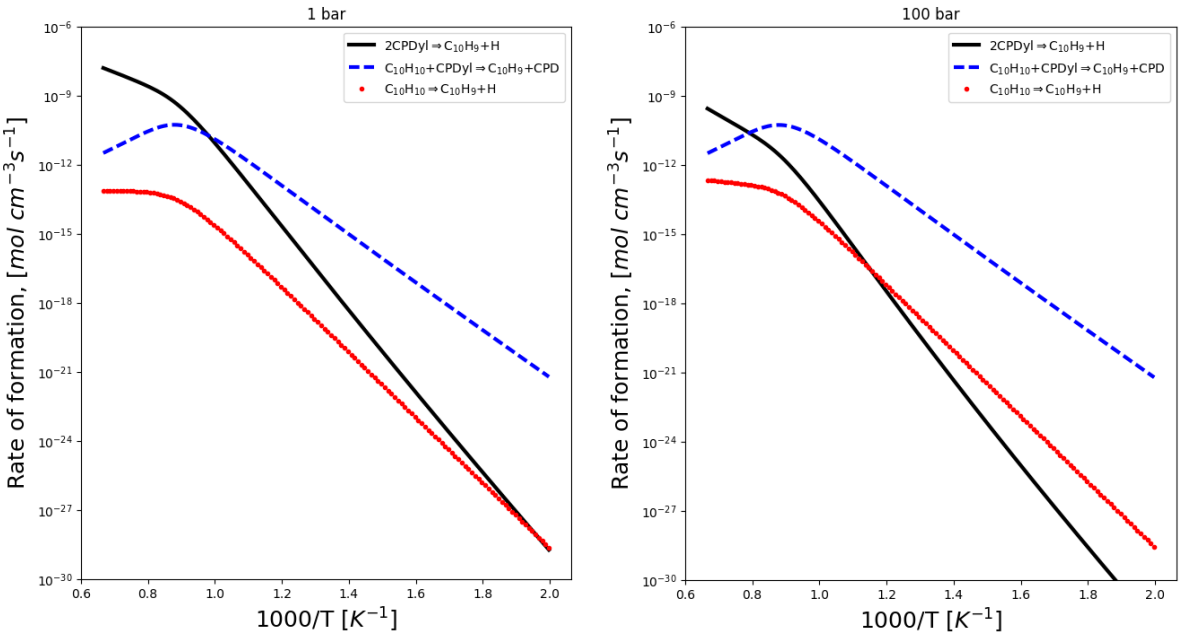

Figure 6: *Rate of $C_{10}H_9$ formation comparison between hydrogen emission from the CPDyl dimer, chemically activated hydrogen emission from the CPDyl + CPDyl reaction, and radical hydrogen abstraction from the CPDyl dimer. At moderate to low temperatures, radical abstraction dominates while at high temperatures the activated path leads formation of $C_{10}H_9$.* [Color: web only]

3.2 $C_{10}H_9$ PES to Azulene and Naphthalene

The direct spiran path from the fulvalanyl radical to naphthalene used here (Figure 7) is consistent with the one originally shown by Melius et al. The surface was subsequently re-calculated at the B3LYP/6-31G(d,p) level of theory by Wang et al. as well as Kislov and Mebel who include this route as part of a larger study[38,39]. In the current study, CBS-QB3 based energies are used. Based on the discussion above, the low-lying $C_{10}H_9$ species **N1b** is formed most rapidly. However, H atom scrambling in species **N1b** is fast and leads to the formation of its isomers **N1a** and **N1c**. Species **N1c** can undergo a 1,3-cycloaddition leading to species **N2**. β-scission of this component leads to the spirane-type species **N3**. This component then reacts via a 1,3-cycloaddition and β-scission to species **N5**, which yields naphthalene by β-scission of a C–H bond.

Though the azulane species are not generally observed to be the dominant product on the $C_{10}H_{10}$ PES at the conditions discussed in this study, the Cavallotti et al. publication adds relevance for azulanyl radical conversion to naphthalene in addition to the route from

fulvalanyl radicals. Routes between azulene and naphthalene were previously explored by Alder et al. who found two dominant options: the spiran path, and the methylene walk route[44]. Entrance channels for the methylene walk path were observed to be significantly higher than for the spiran route, and thus the methylene walk route has been neglected here. This is in agreement with the expectations of Cavallotti et al. who proposed the spiran route to follow from the azulanyl formation shown in their study. As might be expected, the Alder spiran path merges with the Melius spiran route from fulvalanyl to naphthalene. This occurs at species **N4** and the combined surfaces are shown in Figure 7.

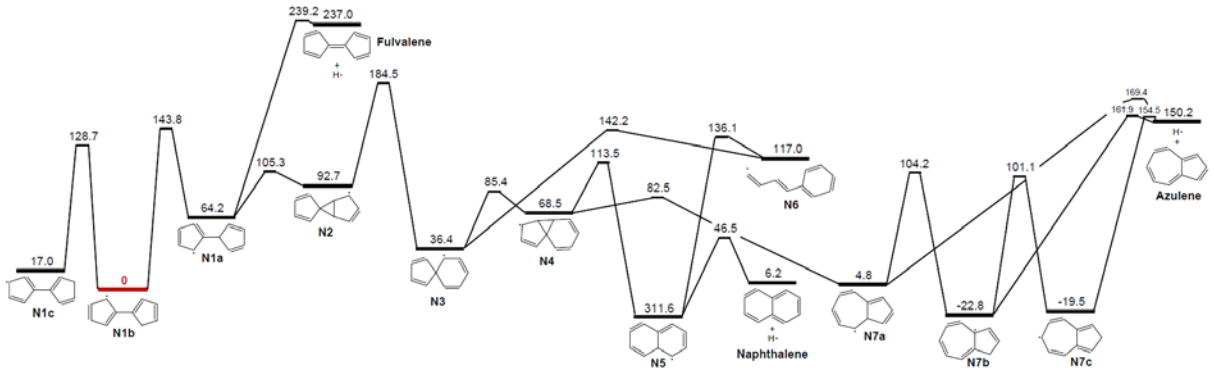

Figure 7: *CBS-QB3 enthalpy diagram H(0 K) (kJ mol^{-1}) on the $C_{10}H_9$ surface leading to the formation of naphthalene and azulene. All enthalpies are relative to component* ***N1b*** . [Color: web only]

Considering the $C_{10}H_9$ PES shown in Figure 7, the pressure-dependent rates shown in Figure 8 are computed. The primary entrance species, **N1b**, equilibrates with the other fulvalanyl isomers **N1a** and **N1c** on a sub-microsecond timescale. The bottleneck on this PES is the ring opening reaction **N2→N3**, passing over a 90 kJ/mol barrier. Interestingly, after passing through species **N2**, the $C_{10}H_9$ species is predicted to pass through the azulanyl species before proceeding on to naphthalene. Since bimolecular reactions are observed to be of relevance for $C_{10}H_{10}$, the lifetime of the $C_{10}H_9$ species is determined by simulating the $C_{10}H_9$ sub-mechanism using CHEMKIN. When starting with an initial concentration of **N1b**, the formation of $C_{10}H_8$ (overwhelmingly naphthalene) follows an exponential curve. This gives $C_{10}H_9$ half-lives of about 20 ms at 800 K, and 20 µs at 1200 K, for a pressure of 1 bar. At these lifetimes bimolecular reaction rates between $C_{10}H_9$ and other species are expected to be relevant, diverting away from naphthalene formation and on to higher carbon number and other species. For example, in combustion systems $C_{10}H_9 + O_2$ reactions are expected to be especially relevant. Rate based automated mechanism generators such as RMG consider all

feasible elementary reactions and will – if necessary – include automatically important bimolecular reactions for $C_{10}H_9$ during mechanism generation.

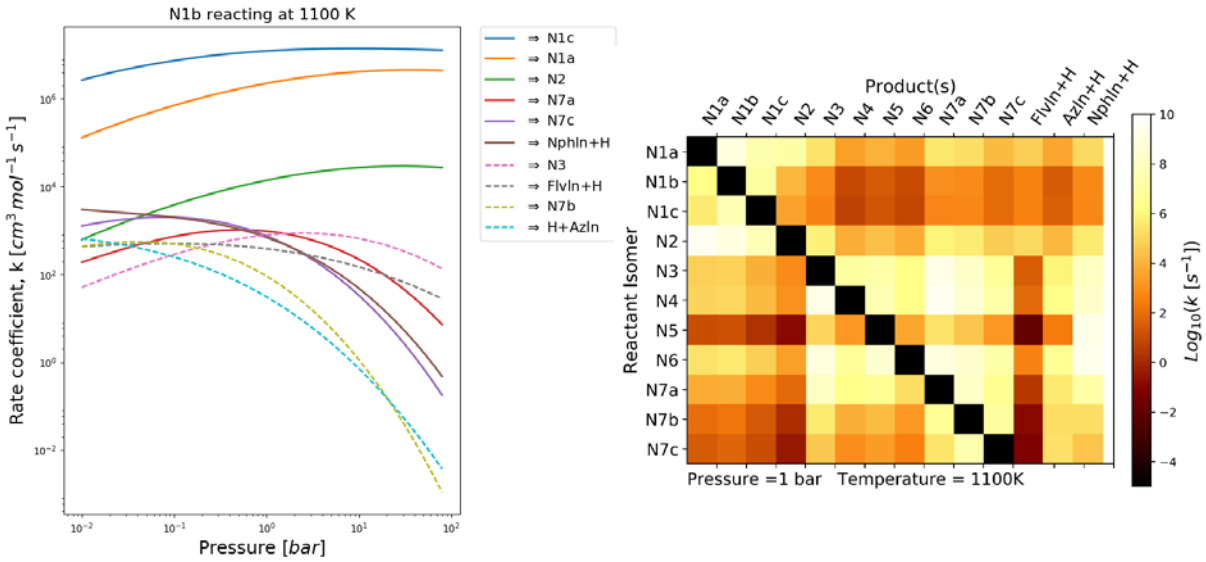

Figure 8*: (**A**: Left) Computed pressure dependent rate coefficients for the species N1b, the primary entrance channel to the $C_{10}H_9$ surface to form various products at 1100K in N_2. The corresponding PES is shown in Figure 7. (**B**: Right) Rate constant matrix for well-skipping and direct reactions among the isomers of the $C_{10}H_9$ PES. Reacting species shown on the y axis with the product species along the x axis. [Flvln = fulvalene, Azln = azulene, Nphln = naphthalene]* [Color: web & print]

4 Conclusions

In this study, a pressure-dependence analysis of the CPDyl + CPDyl recombination reaction and subsequent reactions leading to naphthalene is provided. At all low to intermediate temperature conditions (up to 1020K at 1 bar and 1230K at 100 bar), naphthalene is mainly formed via a series of reaction steps starting with the formation of $C_{10}H_{10}$ isomers and not through the direct chemically activated reaction $C_5H_5+C_5H_5 \rightarrow C_{10}H_8+H+H$. The addition of deeper wells to the $C_{10}H_{10}$ potential energy surface from the Cavallotti et al. work shifts the equilibrium of the cyclopentadienyl recombination reaction more to the right and allows the $C_{10}H_{10}$ species to accumulate more than predicted from the truncated potential energy surface used by Melius et al. and Kislov and Mebel[37,39]. Since C-H scission of any $C_{10}H_{10}$ isomer is highly endothermic, the $C_{10}H_{10}$ species are predicted to accumulate to high concentrations which enables bimolecular hydrogen abstraction reactions to become competitive. $C_{10}H_9$ formation through H abstraction is expected to be the preferred route at pyrolytic conditions at 1 bar and temperatures below 1020K. H abstraction is predicted to be even more important at higher pressures. The net effect of this analysis is that at low to intermediate temperatures

naphthalene formation via CPDyl recombination consumes three radicals (two CPDyl and one abstracting radical (or atom)) while just one H atom is produced. This is in stark contrast to the simplified scheme ($C_5H_5+C_5H_5 \rightarrow C_{10}H_8+H+H$), which implies that naphthalene formation goes along with the conversion of two relatively stable CPDyl radials to two more reactive H atoms. Therefore the reaction pathways are summarized as:

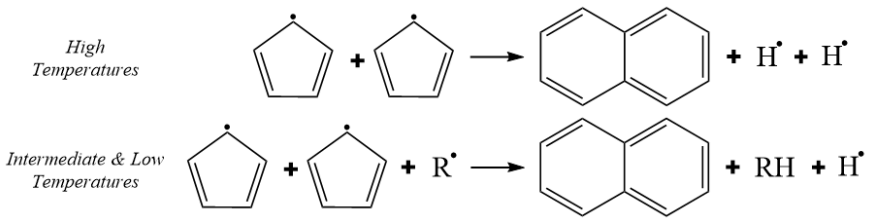

Isomerizations on the $C_{10}H_9$ surface directly to naphthalene are considered as well as those that pass through the formation of the azulanyl radical. This work indicates that $C_{10}H_9$ intermediates will be collisionally stabilized and live for a period of roughly 20 μs at 1200K and 1 bar before decomposing to $C_{10}H_8+H$. Pressure dependent rate coefficients in CHEMKIN compatible format are given in Supplementary Materials for use in future kinetic modeling studies.

The formation of the first PAHs is a complex process that involves many intermediates and reactions. The growth to larger PAHs, such as anthracene and phenanthrene, would require many more possible intermediates and reactions and might prove too complex to study manually. Automated network generators, such as RMG, and automatic reaction discovery are hence indispensable in order to unravel the important steps in the growth of PAHs[49,73]. Studies such as this one help to provide the integral theoretic backbone on which automatic software operates when predicting more complex chemistries. Future work should try to address the growth to tri- and tetracyclic PAHs through automated means.

Acknowledgements

AGV and SSM acknowledge financial support by the Combustion Energy Frontier Research Center, funded by the U.S. Department of Energy, Office of Basic Energy Sciences under award number DE-SC0001198. AEL and WHG acknowledge financial support from the DOE Gas Phase Chemical Physics program, grant No. DE-SC0014901. HHC, AJV, GBM, and KVG acknowledge financial support from the Research Board of Ghent University (BOF),

the 'Long Term Structural Methusalem Funding by the Flemish Government', the European Research Council under the European Union’s Seventh Framework Programme (FP7/2007-2013) / ERC grant agreement n° 290793, the IWT SBO-Project BIOLEUM, and ARBOREF. This research used resources of the National Energy Research Scientific Computing Center under Contract No. DE-AC02-05CH11231.

References

[1] G. Liu, Z. Niu, D. Van Niekerk, J. Xue, L. Zheng, Polycyclic aromatic hydrocarbons (PAHs) from coal combustion: Emissions, analysis, and toxicology, Rev. Environ. Contam. Toxicol., 192 (2008) 1–28.

[2] P. Brookes, Mutagenicity of polycyclic aromatic hydrocarbons, Mutat. Res., 39 (1977) 257–283.

[3] S. Broyde, B. Hingerty, Mutagenicity of Polycyclic Aromatic Hydrocarbons and Amines: A Conformational Hypothesis, Ann. N. Y. Acad. Sci., 435 (1984) 119–122.

[4] K.-H. Kim, S.A. Jahan, E. Kabir, R.J.C. Brown, A review of airborne polycyclic aromatic hydrocarbons (PAHs) and their human health effects, Environ. Int., 60 (2013) 71–80.

[5] B.J. Finlayson-Pitts, J.N. Pitts, Tropospheric air pollution: ozone, airborne toxics, polycyclic aromatic hydrocarbons, and particles, Science, 276 (1997) 1045–1052.

[6] Y.-C. Lin, P.-M. Yang, C.-B. Chen, Reducing Emissions of Polycyclic Aromatic Hydrocarbons and Greenhouse Gases from Engines Using a Novel Plasma-Enhanced Combustion System, Aerosol Air Qual. Res., 13 (2013) 1107–1115.

[7] M.S. Callén, M.T. de la Cruz, S. Marinov, R. Murillo, M. Stefanova, A.M. Mastral, Flue gas cleaning in power stations by using electron beam technology Influence on PAH emissions, Fuel Process. Technol., 88 (2007) 251–258.

[8] J.H. Johnson, S.T. Bagley, L.D. Gratz, D.G. Leddy, A Review of Diesel Particulate Control Technology and Emissions Effects - 1992 Horning Memorial Award Lecture, SAE Tech. Pap., (1994) 940233.

[9] G.P. Smith, D.M. Golden, M. Frenklach, N.W. Miriaty, B. Eiteneer, M. Goldenberg, T. Bowman, R.K. Hanson, S. Song, W.C. Gardiner, V. Lissianski, Z. Qin, GRImech30, (2000).

[10] H. Wang, X. You, A. V Joshi, S.G. Davis, A. Laskin, F.N. Egolfopoulos, C.K. Law, USC Mech Version II: High Temperature Combustion Reaction Model of H2/CO/C1-C4 Compounds, (2007).

[11] Y. Li, C.-W. Zhou, U. Burke, S. Burke, M. Metcalfe, A. Keromnes, H.J. Curran, AramcoMech20, (2016).

[12] M. Frenklach, H. Wang, Detailed modeling of soot particle nucleation and growth, Symp. Combust., 23 (1991) 1559–1566.

[13] J. Appel, H. Bockhorn, M. Frenklach, Kinetic modeling of soot formation with detailed chemistry and physics: laminar premixed flames of C2 hydrocarbons, Combust. Flame, 121 (2000) 122–136.

[14] H. Richter, J.B. Howard, Formation of polycyclic aromatic hydrocarbons and their growth to soot-a review of chemical reaction pathways, Prog. Energy Combust. Sci., 26 (2000) 565–608.

[15] H. Richter, S. Granata, W.H. Green, J.B. Howard, Detailed modeling of PAH and soot formation in a laminar premixed benzene/oxygen/argon low-pressure flame, Proc. Combust. Inst., 30 (2005) 1397–1405.

[16] N. Hansen, W. Li, M.E. Law, T. Kasper, P.R. Westmoreland, B. Yang, T.A. Cool, A.

Lucassen, The importance of fuel dissociation and propargyl + allyl association for the formation of benzene in a fuel-rich 1-hexene flame, Phys. Chem. Chem. Phys., 12 (2010) 12112.

[17] J.A. Miller, C.F. Melius, Kinetic and thermodynamic issues in the formation of aromatic compounds in flames of aliphatic fuels, Combust. Flame, 91 (1992) 21–39.

[18] J.A. Miller, S.J. Klippenstein, The recombination of propargyl radicals: Solving the master equation, J. Phys. Chem. A, 105 (2001) 7254–7266.

[19] Z. Wang, L. Zhao, Y. Wang, H. Bian, L. Zhang, F. Zhang, Y. Li, S.M. Sarathy, F. Qi, Kinetics of ethylcyclohexane pyrolysis and oxidation: An experimental and detailed kinetic modeling study, Combust. Flame, 162 (2015) 2873–2892.

[20] A.M. Scheer, C. Mukarakate, D.J. Robichaud, G.B. Ellison, M.R. Nimlos, Radical Chemistry in the Thermal Decomposition of Anisole and Deuterated Anisoles: An Investigation of Aromatic Growth, J. Phys. Chem. A, 114 (2010) 9043–9056.

[21] A.B. Lovell, K. Brezinsky, I. Glassman, The gas phase pyrolysis of phenol, Int. J. Chem. Kinet., 21 (1989) 547–560.

[22] J.K. McDonald, J.A. Merritt, B.J. Alley, S.P. McManus, Gas-phase thermolysis of 1,5-hexadiene: the continuous wave carbon dioxide laser-induced reaction and studies of the cyclization pathway, J. Am. Chem. Soc., 107 (1985) 3008–3012.

[23] T.R. Melton, F. Inal, S.M. Senkan, The effects of equivalence ratio on the formation of polycyclic aromatic hydrocarbons and soot in premixed ethane flames, Combust. Flame, 121 (2000) 671–678.

[24] M. Szwarc, The Determination Of Bond Dissociation Energies By Pyrolytic Methods, Chem. Rev., 47 (1950) 75–173.

[25] R. Spielmann, C.A. Cramers, Cyclopentadienic compounds as intermediates in the thermal degradation of phenols Kinetics of the thermal decomposition of cyclopentadiene, Chromatographia, 5 (1972) 295–300.

[26] R. Cypres, B. Bettens, La formation de la plupart des composes aromatiques produits lors de la pyrolyse du phenol, ne fait pas intervenir le carbone porteur de la fonction hydroxyle, Tetrahedron, 31 (1975) 359–365.

[27] R. Cypres, B. Bettens, Mecanismes de fragmentation pyrolytique du phenol et des cresols, Tetrahedron, 30 (1974) 1253–1260.

[28] J.A. Manion, R. Louw, Rates, products, and mechanisms in the gas-phase hydrogenolysis of phenol between 922 and 1175 K, J. Phys. Chem., 93 (1989) 3563–3574.

[29] K. Roy, M. Braun-Unkhoff, P. Frank, T. Just, Kinetics of the cyclopentadiene decay and the recombination of cyclopentadienyl radicals with H-atoms: Enthalpy of formation of the cyclopentadienyl radical, Int. J. Chem. Kinet., 33 (2001) 821–833.

[30] K. Roy, P. Frank, T. Just, Shock Tube Study of High-Temperature Reactions of Cyclopentadiene, Isr. J. Chem., 36 (1996) 275–278.

[31] Y. Murakami, T. Saejung, Ic. Ohash, N. Fujii, Investigation of a New Pathway Forming Naphthalene by the Recombination Reaction of Cyclopentadienyl Radicals, Chem. Lett., 32 (2003) 1112–1113.

[32] D.H. Kim, J.A. Mulholland, D. Wang, A. Violi, Pyrolytic hydrocarbon growth from

cyclopentadiene, J. Phys. Chem. A, 114 (2010) 12411–12416.

[33] M.R. Djokic, K.M. Van Geem, C. Cavallotti, A. Frassoldati, E. Ranzi, G.B. Marin, An experimental and kinetic modeling study of cyclopentadiene pyrolysis: First growth of polycyclic aromatic hydrocarbons, Combust. Flame, 161 (2014) 2739–2751.

[34] A. V. Friderichsen, E.-J. Shin, R.J. Evans, M.R. Nimlos, D.C. Dayton, G.B. Ellison, The pyrolysis of anisole (C6H5OCH3) using a hyperthermal nozzle, Fuel, 80 (2001) 1747–1755.

[35] M. Djokic, H.-H. Carstensen, K.M. Van Geem, G.B. Marin, The thermal decomposition of 2,5-dimethylfuran, Proc. Combust. Inst., 34 (2013) 251–258.

[36] V.D. Knyazev, K. V. Popov, Kinetics of the Self Reaction of Cyclopentadienyl Radicals, J. Phys. Chem. A, 119 (2015) 7418–7429.

[37] C.F. Melius, M.E. Colvin, N.M. Marinov, W.J. Pit, S.M. Senkan, Reaction mechanisms in aromatic hydrocarbon formation involving the C5H5 cyclopentadienyl moiety, Symp. Combust., 26 (1996) 685–692.

[38] D. Wang, A. Violi, D.H. Kim, J.A. Mullholland, Formation of naphthalene, indene, and benzene from cyclopentadiene pyrolysis: A DFT study, J. Phys. Chem. A, 110 (2006) 4719–4725.

[39] V. V Kislov, A.M. Mebel, An ab initio G3-type/statistical theory study of the formation of indene in combustion flames II The pathways originating from reactions of cyclic C 5 species-cyclopentadiene and cyclopentadienyl radicals, J. Phys. Chem. A, 112 (2008) 700–716.

[40] A.M. Mebel, V. V Kislov, Can the C5H5 + C5H5 ->C10H10 ->C10H9 + H/C10H8 + H2 reaction produce naphthalene? An ab initio/RRKM study, J. Phys. Chem. A, 113 (2009) 9825–9833.

[41] A.M. Dean, Detailed Kinetic Modeling of Autocatalysis in Methane Pyrolysis, J. Phys. Chem., 94 (1990) 1432–1439.

[42] C. Cavallotti, D. Polino, A. Frassoldati, E. Ranzi, Analysis of some reaction pathways active during cyclopentadiene pyrolysis, J. Phys. Chem. A, 116 (2012) 3313–3324.

[43] C. Cavallotti, D. Polino, On the kinetics of the C5H5+C5H5 reaction, Proc. Combust. Inst., 34 (2013) 557–564.

[44] R.W. Alder, S.P. East, J.N. Harvey, M.T. Oakley, The azulene-to-naphthalene rearrangement revisited: A DFT study of intramolecular and radical-promoted mechanisms, J. Am. Chem. Soc., 125 (2003) 5375–5387.

[45] A.M. Mebel, A. Landera, R.I. Kaiser, Formation Mechanisms of Naphthalene and Indene: From the Interstellar Medium to Combustion Flames, J. Phys. Chem. A, 121 (2017) 901–926.

[46] V. V. Kislov, A.M. Mebel, The formation of naphthalene, azulene, and fulvalene from cyclic C 5 species in combustion: An ab initio/RRKM study of 9-H-fulvalenyl (C 5H 5-C 5H 4) radical rearrangements, J. Phys. Chem. A, 111 (2007) 9532–9543.

[47] B.M. Wong, D.M. Matheu, W.H. Green, Temperature and molecular size dependence of the high-pressure limit, J. Phys. Chem. A, 107 (2003) 6206–6211.

[48] K. Wang, S.M. Villano, A.M. Dean, Fundamentally-based kinetic model for propene pyrolysis, Combust. Flame, 162 (2015) 4456–4470.

[49] C.W. Gao, J.W. Allen, W.H. Green, R.H. West, Reaction Mechanism Generator: Automatic construction of chemical kinetic mechanisms, Comput. Phys. Commun., 203 (2016) 212–225.

[50] J.A. Montgomery, M.J. Frisch, J.W. Ochterski, G.A. Petersson, A complete basis set model chemistry VI Use of density functional geometries and frequencies, J. Chem. Phys., 110 (1999) 2822–2827.

[51] J.J.A. Montgomery, M.J. Frisch, J.W. Ochterski, G.A. Petersson, A complete basis set model chemistry VII Use of the minimum populationlocalization method, J. Chem. Phys., 112 (2000) 6532.

[52] M.J. Frisch, G.W. Trucks, H.B. Schlegel, G.E. Scuseria, M.A. Robb, J.R. Cheeseman, J.A. Montgomery, T. Vreven, K.N. Kudin, J.C. Burant, J.M. Millam, S.S. Iyengar, J. Tomasi, V. Barone, B. Mennucci, M. Cossi, G. Scalmani, N. Rega, G.A. Petersson, H. Nakatsuji, et al., Gaussian 03, (2003) Distributed by GAUSSIAN, Inc.

[53] M.J. Frisch, G.W. Trucks, H.B. Schlegel, G.E. Scuseria, M.A. Robb, J.R. Cheeseman, G. Scalmani, V. Barone, B. Mennucci, G.A. Petersson, H. Nakatsuji, M. Caricato, X. Li, H.P. Hratchian, A.F. Izmaylov, J. Bloino, G. Zheng, J.L. Sonnenberg, M. Hada, M. Ehara, et al., Gaussian 09, (2009) Distributed by GAUSSIAN, Inc.

[54] P.D. Paraskevas, M.K. Sabbe, M.F. Reyniers, N. Papayannakos, G.B. Marin, Group additive values for the gas-phase standard enthalpy of formation, entropy and heat capacity of oxygenates, Chem. - A Eur. J., 19 (2013) 16431–16452.

[55] C. Moore, Atomic energy levels as derived from the analyses of optical spectra, US Dept. of Commerce, National Bureau of Standards, 1949.

[56] K.S. Pitzer, W.D. Gwinn, Energy Levels and Thermodynamic Functions for Molecules with Internal Rotation I Rigid Frame with Attached Tops, J. Chem. Phys., 10 (1942) 428.

[57] C. Eckart, The penetration of a potential barrier by electrons, Phys. Rev., 35 (1930) 1303–1309.

[58] R.A. Marcus, O.K. Rice, The Kinetics of the Recombination of Methyl Radicals and Iodine Atoms, J. Phys. Chem., 55 (1951) 894–908.

[59] O.K. Rice, H.C. Ramsperger, Theories of unimolecular gas reactions at low pressures, J. Am. Chem. Soc., 49 (1927) 1617–1629.

[60] L.S. Kassel, Studies in Homogeneous Gas Reactions I, J. Phys. Chem., 32 (1928) 225–242.

[61] W. Forst, Z. Prasil, Comparative Test of Approximations for Calculation of Energy-Level Densities, J. Chem. Phys., 51 (1969) 3006.

[62] M.R. Hoare, T.W. Ruijgrok, Inversion of the Partition Function: The First-Order Steepest-Descent Method, J. Chem. Phys., 52 (1970) 113–120.

[63] M.R. Hoare, Inversion of the Partition Function II The Full Steepest-Descent Method, J. Chem. Phys., 52 (1970) 5695–5699.

[64] A.Y. Chang, J.W. Bozzelli, A.M. Dean, Kinetic analysis of complex chemical activation and unimolecular dissociation reactions using QRRK theory and the modified strong collision approximation, Zeitschrift Fur Phys. Chemie, 214 (2000) 1533–1568.

[65] J.W. Allen, C.F. Goldsmith, W.H. Green, Automatic estimation of pressure-dependent rate coefficients, Phys. Chem. Chem. Phys., 14 (2012) 1131.

[66] H. Hippler, B. Otto, J. Troe, Collisional Energy Transfer of Vibrationally Highly Excited Molecules VI Energy Dependence of $\langle \Delta E \rangle$ in Azulene, Berichte Der Bunsengesellschaft Für Phys. Chemie, 93 (1989) 428–434.

[67] K.G. Joback, A unified approach to physical property estimation using multivariate statistical techniques MS thesis, MIT, 1984.

[68] J.R. Welty, C.E. Wicks, G. Rorrer, R.E. Wilson, Fundamentals of momentum, heat, and mass transfer, John Wiley & Sons, 2009.

[69] M.R. Harper, K.M. Van Geem, S.P. Pyl, G.B. Marin, W.H. Green, Comprehensive reaction mechanism for n-butanol pyrolysis and combustion, Combust. Flame, 158 (2011) 16–41.

[70] J.W. Allen, S. Sharma, M.R. Harper, W.H. Green, CANTHERM, (2010) rmg.mit.edu.

[71] L.B. Harding, Y. Georgievskii, S.J. Klippenstein, Predictive theory for hydrogen atom-hydrocarbon radical association kinetics, J. Phys. Chem. A, 109 (2005) 4646–4656.

[72] S.J. Blanksby, G.B. Ellison, Bond dissociation energies of organic molecules, Acc. Chem. Res., 36 (2003) 255–263.

[73] Y. V Suleimanov, W.H. Green, Automated Discovery of Elementary Chemical Reaction Steps Using Freezing String and Berny Optimization Methods, J. Chem. Theory Comput., 11 (2015) 4248–4259.

Supporting Information:

- Detailed pressure dependent reaction networks (CHEMKIN format) for each of the surfaces included in separate file.

- Species optimized geometries used in this study included in separate file.

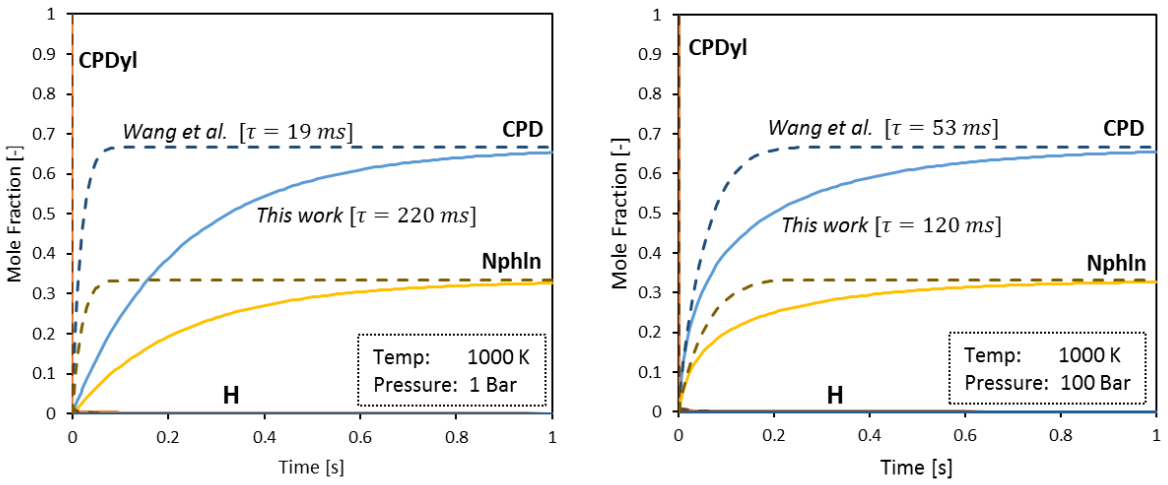

Fig. S1: Comparative analysis between the pressure dependent reaction network calculated in this work and that which was estimated by Wang et al. [48]. Comparison was achieved by simulating the behavior of each sub-mechanism using a Chemkin homogenous reactor module and starting the simulation entirely with CPDyl. The CPD = CPDyl + H reaction was included to allow for consumption of H and a reasonable formation of naphthalene. The network presented in this work is roughly an order of magnitude slower than that of Wang et al at atmospheric pressure and roughly a factor of 2 slower at 100 bar. The opposing pressure trends are attributed to the importance of CPDyl H-abstraction discussed in this work which was not included in the Wang model.

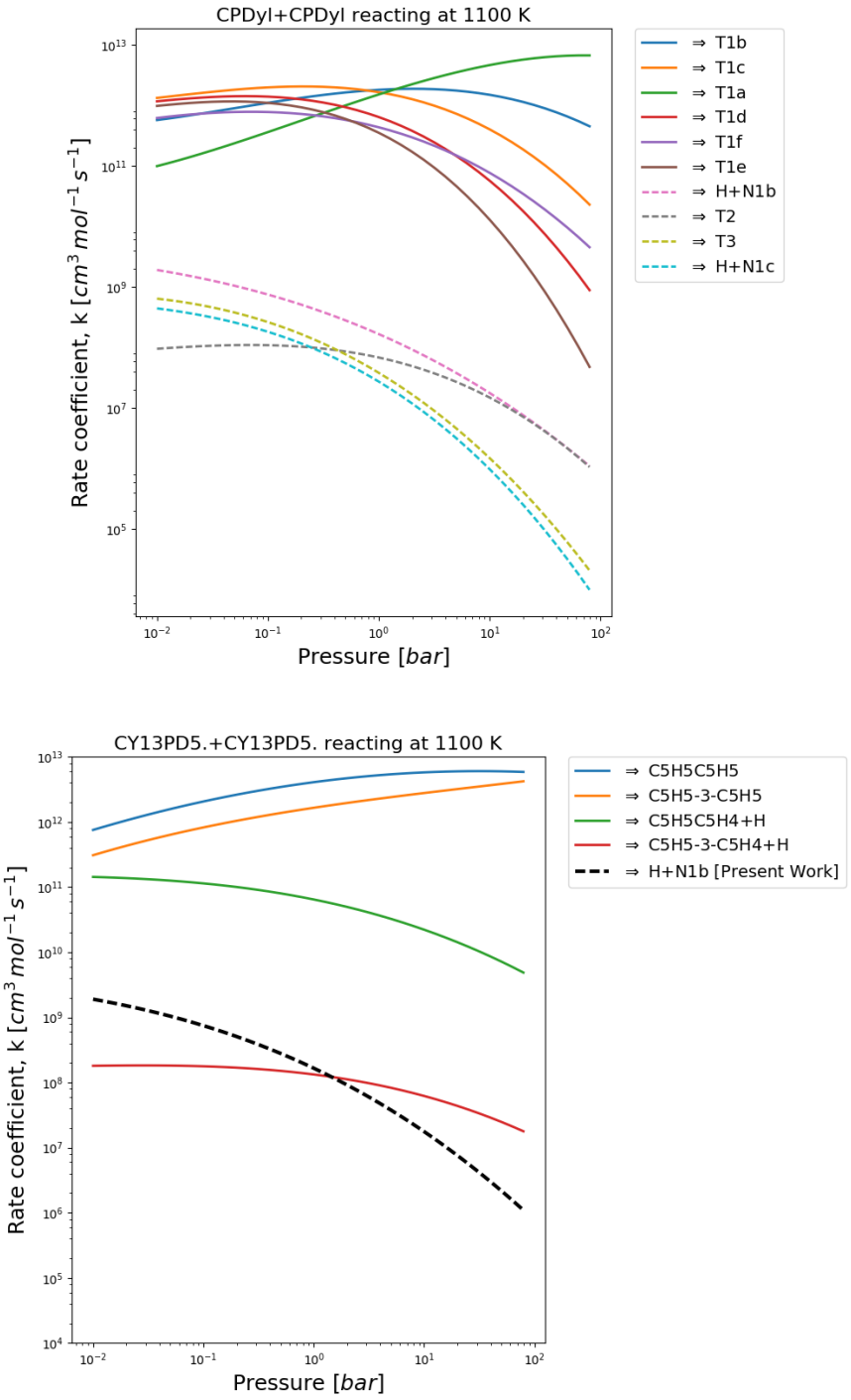

Fig. S2: Reproduction of Figure 5A from this paper (TOP) compared with an analogous figure created from the Wang et al. [48] estimated pressure dependent network rates (BOTTOM). The two networks are observed to be consistent in their high pressure limit rate for CPDyl + CPDyl, but the estimated Wang et al. network shows a significantly higher rate for the chemically activated pathway to $C_{10}H_9 + H$.

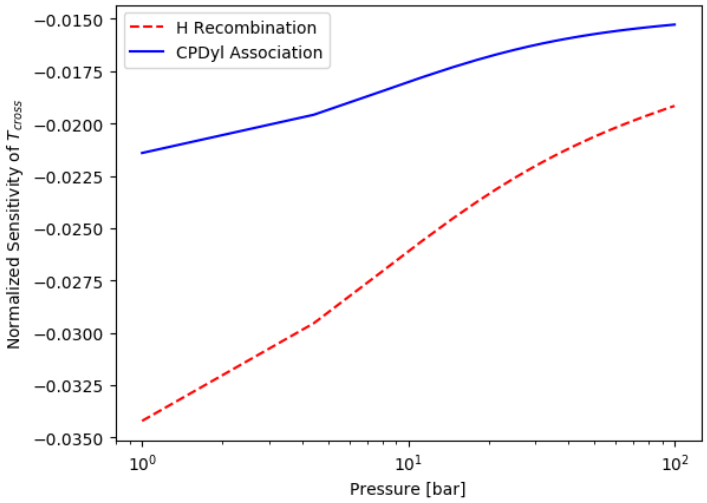

Fig. S3: Brute force sensitivity analysis $\left(s = \frac{A_i}{T_{cross,i}} \frac{\Delta T_{cross}}{\Delta A}\right)$ for the crossover temperature at which the chemically activated rate, 2 CPDyl = $C_{10}H_9$ + H becomes the dominant route to the $C_{10}H_9$ surface. An increase in either rate will lead to a lower T_{cross} with the hydrogen recombination rate having the stronger effect. Both sensitivities are low.

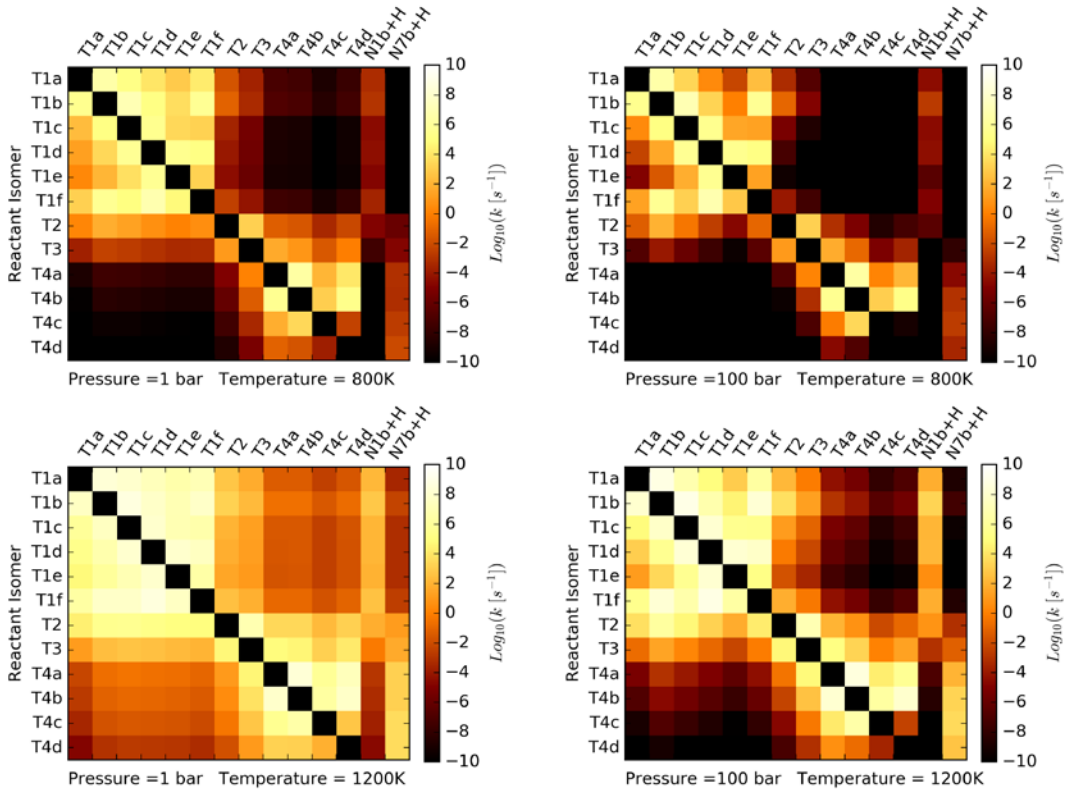

Fig. S4: Isomerization rate constant matrices for the $C_{10}H_{10}$ surface at varying temperature and pressure.

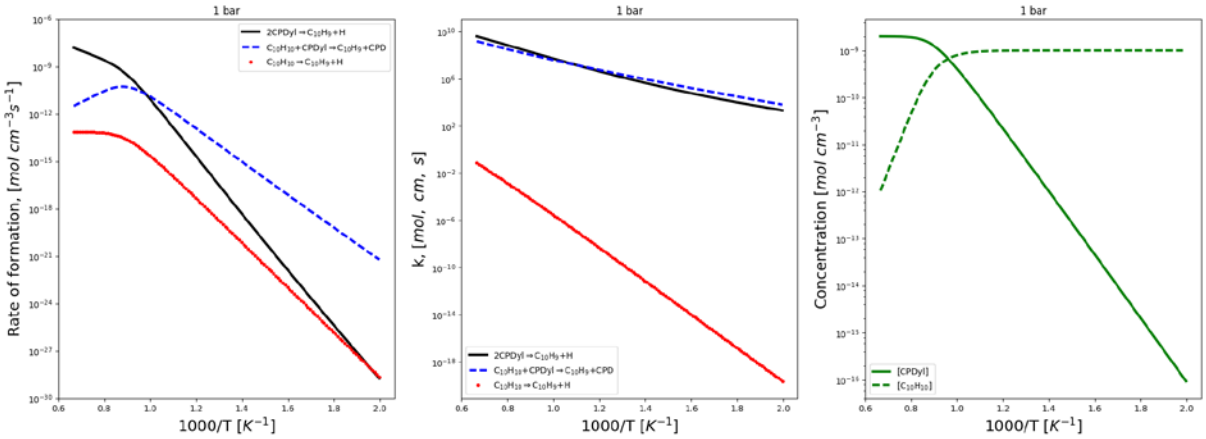

Fig. S5: Factor breakdown of the $C_{10}H_9$ rate of formation plot shown in Figure 6. Changes in slopes for the left most plot are attributed to a shift in the assumed equilibrium between the $C_{10}H_{10}$ species and CPDyl shown in the right most concentration plot.

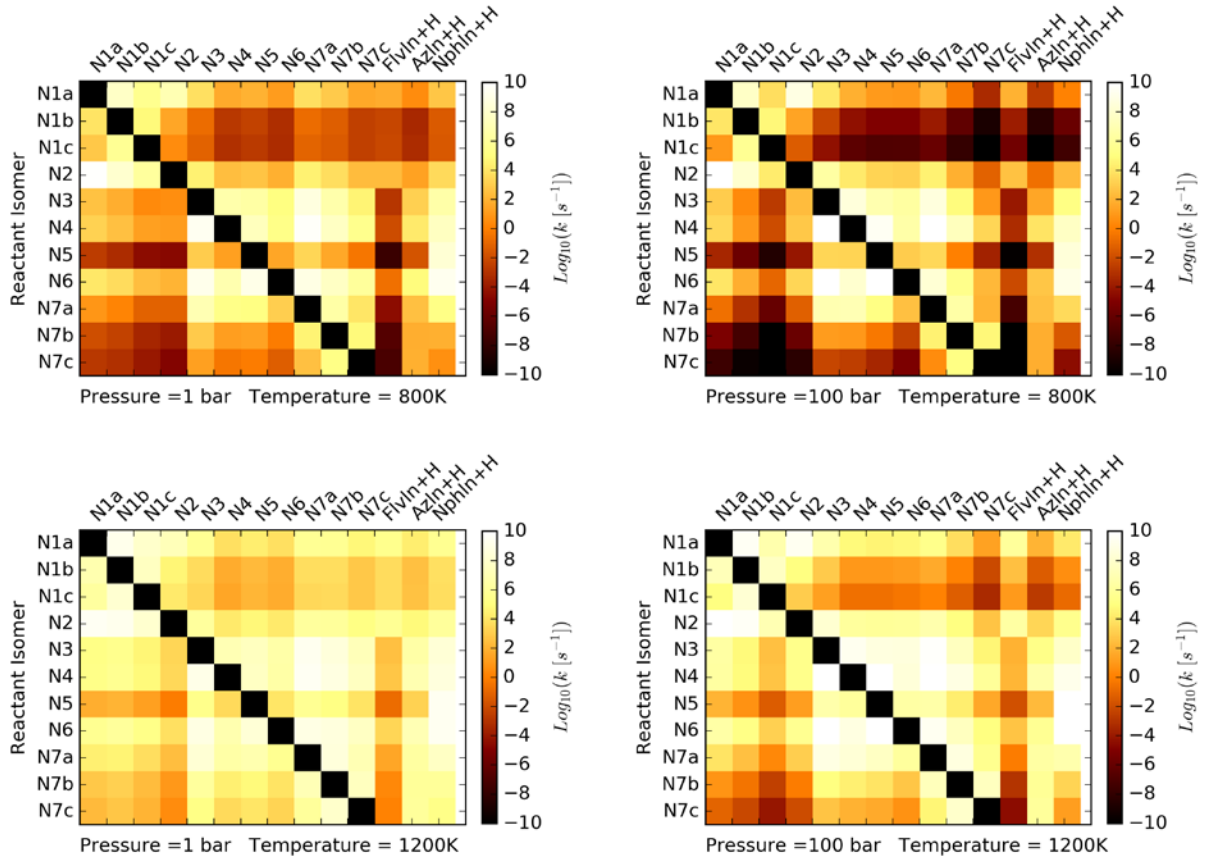

Fig. S6: Isomerization rate constant matrices for the $C_{10}H_9$ surface at varying temperature and pressure.